Functional window of the avian compass

Vishvendra Singh Poonia,[1] Kiran Kondabagil,[2] Dipankar Saha,[1] and Swaroop Ganguly[1,*]
[1]*Department of Electrical Engineering, Indian Institute of Technology Bombay, Mumbai 400076, India*
[2]*Department of Biosciences and Bioengineering, Indian Institute of Technology Bombay, Mumbai 400076, India*
(Received 2 August 2016; revised manuscript received 3 March 2017; published 26 May 2017)

The functional window is an experimentally observed property of the avian compass that refers to its selectivity around the geomagnetic-field strength. We show that the simple radical-pair model, using biologically feasible hyperfine parameters, can qualitatively explain the salient features of the avian compass as observed in behavioral experiments: its functional window, as well as disruption of the compass action by radio-frequency fields of specific frequencies. Further, we show that adjustment of the hyperfine parameters can tune the functional window, suggesting a possible mechanism for its observed adaptation to field variation. While these lend support to the radical-pair model, we find that in its simplest form—or even with minor augmentations—it cannot quantitatively explain the observed width of the functional window. This suggests deeper generalization of the model, possibly in terms of more nuclei or more subtle environmental interaction than has been considered hitherto. Finally, we examine a possible biological purpose for the functional window; even assuming evolutionary benefit from radical-pair magnetoreception, it seems likely that the functional window could be just a corollary thereof, imparting no additional advantage.

DOI: 10.1103/PhysRevE.95.052417

I. INTRODUCTION

Avian magnetoreception—the ability of some bird species to navigate by sensing (the earth's) magnetic field—is one of a set of "quantum biological" phenomena [1–10] in which nontrivial quantum effects are thought to play an overt functional role even under warm, dirty conditions [11–16]. An understanding of these phenomena could point the way towards engineering room-temperature quantum biomimetic or quantum information systems.

The radical-pair (RP) model of the avian compass hinges on the dynamics of electron spins on a photoexcited radical pair. These spins can be in the singlet or triplet states (or a superposition thereof) before the radicals recombine. The fraction of recombination product obtained from radical pairs in the singlet state is called the singlet yield, which acts as a measure of the geomagnetic field inclination. The RP model has been successful in explaining several of the observed behavioral characteristics [11,17]. These include photoinitiated operation [11], dependence on the inclination and not the polarity of the geomagnetic field [11], and disruption by radio-frequency (RF) fields [18–21]. The RP recombination time is thus estimated to be of the order of microseconds [14,16,22]; the coherence time, which should be longer than this recombination time in order for the geomagnetic field to exercise an appreciable effect on the RP spin dynamics, is thus expected to be in the tens of microseconds. It is the long coherence time in a noisy environment that makes this system especially intriguing. The compass action also happens to be extremely sensitive to small RF fields of 1.315 MHz [19,20], which happens to be the Larmor frequency of a free electron. This indicates a spin dynamical mechanism for the avian compass in which one of the electron spins is nearly free. (The other electron spin happens to be subjected to a hyperfine interaction, while both of them interact with the geomagnetic Zeeman field.)

There is, however, one characteristic of the avian compass which is not yet completely understood. This is the so-called "functional window" [23–25], which refers to a decrease in the compass sensitivity when the Zeeman-field magnitude is outside of a window centered on the geomagnetic field. Behavioral experiments have found that apart from the local magnetic field of 47 μT, birds are receptive to magnetic fields of 43 and 54 μT; however, they get disoriented for 16, 34, 60, 81, and 150 μT [11]. Moreover, if the bird is exposed to a magnetic-field intensity long enough, its compass gets "trained" and is recentered on the new magnetic field [11,25]. We call this property the "functional window adaptation" of the avian compass. An early indication of the dependence of the compass sensitivity, *viz.*, the singlet yield, on the magnetic field was reported by Rodgers and Hore [26]; later Bandyopadhyay *et al.* [22] analyzed the effect on the compass sensitivity of increasing or decreasing the Zeeman field by 30% [27]. Recently, Xu *et al.* proposed a hyperfine parameter set for the avian compass for which the compass responds to a $\pm$30% change in the ambient magnetic (Zeeman) field and external RF field (1.315 MHz), up to the intensity of 15 nT [28].

In this paper, we show that the windowlike behavior centered at the local geomagnetic field (as well as the RF disruption) emerges from the RP model for a biologically feasible hyperfine parameter set. We started out with a few hundred such parameter sets and narrowed down, first, to those which yield a functional window centered on the geomagnetic field of 47 μT and then, further, to those that result in compass function disruption with a 1.315-MHz RF field. We also show that variation of the hyperfine parameters of the compass can explain the functional window adaptation. Thus, the radical-pair dynamics suggests a possible mechanism for this adaption that is, of course, subject to experimental corroboration. Further, we have shown that the compass properties endure for the biologically feasible parameter set even when we relax the usual—but possibly unrealistic—condition of equal

*sganguly@ee.iitb.ac.in

recombination rates from the singlet and triplet states [29]. The parameter set considered here enables us to predict the range of RP recombination times and, thus, the coherence time of RP spin states—which turns out to be more than 25 μs. We show that the functional window behavior is preserved until the environmental noise rate becomes comparable to the recombination rate ($k = 4 \times 10^4$ s^{-1}). Finally, we explore the possible evolutionary benefit(s) from the functional window in the more general context of such benefits from RP avian magnetoreception itself.

The paper is organized as follows: In Sec. II, we discuss the quantum dynamics of the RP model of the avian compass including the method of its simulation. In Sec. III, we explore the functional window characteristic of the avian compass and analyze the trends it follows when various compass parameters are changed. Additionally, we explore the effect of environmental noise on the functional window. In Sec. IV, we discuss evolutionary aspects of avian magnetoreception and the functional window, as well as limitations of the RP model. In Sec. V, we conclude with an assessment of the RP model as a candidate for explaining the functionality of the avian compass. Finally, we provide a detailed discussion of the radical-pair-model parameter space and the effect of environmental noise in Appendixes A and B, respectively.

II. THE RADICAL-PAIR MODEL

The RP model involves a photogenerated radical pair wherein each radical experiences hyperfine interaction with neighboring nuclei. Both radicals interact with the geomagnetic field and therefore the ensuing spin dynamics of the radical pair is influenced by both Zeeman and hyperfine interactions before radicals recombine. The recombination product of the radical pair depends on the spin state of the radical pair just before the recombination; i.e., singlet and triplet spin states give different, distinguishable chemical products after the radical pair recombines. Also, the biological environment around the radical pair is responsible for dephasing [30]. The product yield after recombination corresponding to singlet or triplet states contains the information about the magnetic field, and both Zeeman and anisotropic hyperfine interactions make it so [31]. In order to study the functional window and other behavioral characteristics of the avian compass, we choose an illustrative RP system wherein only one of the radicals undergoes hyperfine interaction with a nucleus [32,33]. Although much more elaborate modeling would be required to simulate the details of the RP mechanism [16], this model captures the qualitative functionality of the avian compass [14]. The RP Hamiltonian is

$$H = \gamma \mathbf{B} \cdot (\hat{S}_1 + \hat{S}_2) + \hat{I} \cdot \mathbf{A} \cdot \hat{S}_2, \tag{1}$$

where $\hat{S}_1$ and $\hat{S}_2$ are electron spin operators, and $\hat{I}$ is the nuclear spin operator. $\mathbf{A}$ is the hyperfine tensor and can be written as $\mathbf{A} = \mathrm{diag}(a_x,a_y,a_z)$. The geomagentic field is characterized by $\mathbf{B} = B_0(\sin\theta\cos\phi, \sin\theta\sin\phi, \cos\theta)$; B_0 (=47 μT) is the local geomagnetic field at Frankfurt [20] and θ is the magnetic-field orientation with respect to the B_z direction, which is taken along the RP axis. The photogeneration of the radical pair is the starting point of RP spin dynamics and this is taken to be $t = 0$. The radical pair is initially in the singlet state and the nuclear spin state is depolarized [11,14,31,34]. The dynamics of the RP system is simulated using the master equation approach with the quantum toolbox in the python (QuTiP) module [14,31,35]. The RP recombination is modeled via Lindblad operators in the master equation as $P_1 = |S\rangle\langle s, \uparrow|$, $P_2 = |S\rangle\langle s, \downarrow|$, $P_3 = |T_0\rangle\langle t_0, \uparrow|$, $P_4 = |T_0\rangle\langle t_0, \downarrow|$, $P_5 = |T_+\rangle\langle t_+, \uparrow|$, $P_6 = |T_+\rangle\langle t_+, \downarrow|$, $P_7 = |T_-\rangle\langle t_-, \uparrow|$, and $P_8 = |T_-\rangle\langle t_-, \downarrow|$ where the arrows ($|\uparrow\rangle, |\downarrow\rangle$) are the states of the nucleus. The master equation, then, is given as

$$\dot{\rho} = -\frac{i}{\hbar}[H,\rho] + k_s \sum_{i=1}^{2} P_i \rho P_i^\dagger - \frac{1}{2}(P_i^\dagger P_i \rho + \rho P_i^\dagger P_i) + k_t \sum_{i=3}^{8} P_i \rho P_i^\dagger - \frac{1}{2}(P_i^\dagger P_i \rho + \rho P_i^\dagger P_i), \tag{2}$$

where k_s and k_t are the recombination rates corresponding to the singlet and triplet radical pairs. The joint state of the radical pair and nucleus at $t = 0$ is $\rho(0) = \frac{1}{2} I \otimes (|s\rangle \otimes \langle s|)$. The singlet yield is defined as the proportion of recombined chemical product originating from the singlet precursor. The triplet can also be defined similarly. The variation of the singlet yield Φ_S (*viz.*, the fraction of radical pairs recombining from the singlet spin state) with the geomagnetic field inclination leads to compass functionality in the RP model. Most of the following discussion, in fact, is in terms of the compass sensitivity $D_S = \Phi_S^{\max} - \Phi_S^{\min}$, *viz.*, the difference between the maximum and the minimum singlet yield as a function of the inclination [33].

III. THE FUNCTIONAL WINDOW

The functional window is defined as a band-pass-filter-like characteristic wherein the compass sensitivity is appreciable only for a narrow range of magnetic fields and negligible otherwise. In order to locate the functional window, the compass sensitivity as a function of the geomagnetic (Zeeman)-field intensity is analyzed for a large number of hyperfine parameters and RP recombination rates. The sharpest functional window, centered at 47 μT, then obtains for the hyperfine parameter set of $(a_x,a_y,a_z) = (0.345\text{ G}, 0.345\text{ G}, 9\text{ G})$ with $(k_s,k_t) = (2 \times 10^4\text{ s}^{-1}, 2 \times 10^4\text{ s}^{-1})$; this is shown in Fig. 1(a). This parameter set is shown to fall within the biologically feasible regime of hyperfine interaction strength, which ranges from 0.1 to 10 G [26]. Moreover, this set of hyperfine and recombination rate parameters also exhibits the RF disruption property, as shown in Fig. 1(b). The RF field of 1.315 MHz is considered to be disrupting the avian compass functionality if the compass sensitivity drops by more than 30% in the presence of the RF field [22,27]. The singlet yield with and without the RF field is shown in Fig. 1(b) for the aforementioned hyperfine and recombination parameter set, which clearly illustrates the RF disruption of avian compass.

Henceforth, we discuss the the methodology of discovering the functional window and the regime of hyperfine and recombination parameters explored. The z axis is assumed along the RP axis. The hyperfine parameter sets can broadly be divided into two regimes: cigar-shaped ($a_x = a_y < a_z$) and disk-shaped ($a_x = a_y > a_z$), assuming symmetry in the transverse plane. For cigar-shaped hyperfine parameters, we

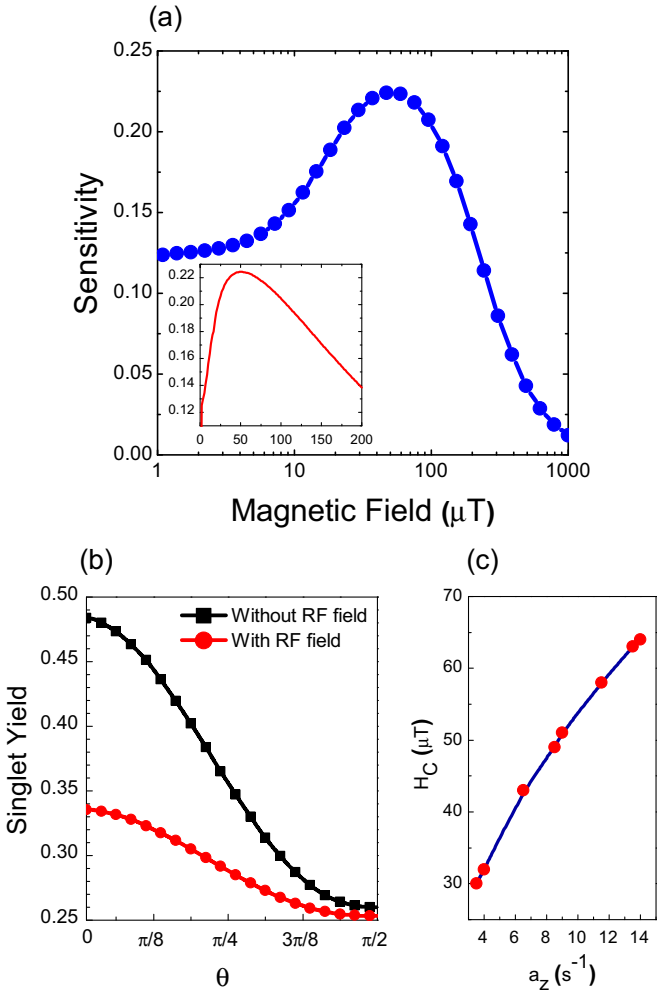

FIG. 1. (a) Compass sensitivity as a function of the Zeeman field for $(a_x,a_y,a_z,k_s,k_t) = (0.345\ \text{G},0.345\ \text{G},9\ \text{G},2\times10^4\ \text{s}^{-1},2\times10^4\ \text{s}^{-1})$. The plot clearly reveals a "functional window" centered around 47 μT. Inset: The functional window, for the linear scale of the magnetic field. (b) Singlet yield as a function of the geomagnetic field inclination for $(a_x,a_y,a_z,k_s,k_t) = (0.345\ \text{G},0.345\ \text{G},9\ \text{G},2\times10^4\ \text{s}^{-1},2\times10^4\ \text{s}^{-1})$ with (red circles) and without (black squares) a 150-nT RF field of 1.315-MHz frequency. The figure distinctly shows the degradation of compass sensitivity in the presence of the RF field, a defining characteristic of the avian compass. (c) Variation of the center of the functional window (denoted H_C) as a function of the axial hyperfine strength (a_z)—indicative of functional window adaptation.

examine a_z values varying from 0 to $100B_{\text{geo}}$ and a_x and a_y are varied from 0 to a_z. Similarly for disk-shaped hyperfine parameters, the values of a_x and a_y are varied from 0 to $100B_{\text{geo}}$ and a_z is varied from 0 to a_x $(=a_y)$. In addition to this, we also explored these two set of hyperfine parameters for the case where $a_x \neq a_y$ but it did not offer any distinctive observation. For these hyperfine parameters, recombination rates (k_s,k_t) from 10^4 to 10^7 s^{-1} were examined. A functional window having a varied width and center at different Zeeman magnetic fields is obtained for many combinations of these parameters and a general trend is observed with respect to the strength of hyperfine parameters and recombination rates. Qualitatively the following things are observed: (a) As the value of a_z increases, the center and width of the functional window shift towards higher values of the Zeeman field. The lower part of the functional window remains still with respect to the change in the value of a_z. (b) a_x and a_y affect only the height of the functional window and not the width. The higher the value of a_x (or a_y), the lower is the height of the functional window. (c) The recombination rate affects the lower limit of the functional window and increasing (decreasing) the recombination rate would shift the lower limit of the functional window towards higher (lower) magnetic-field strengths. However, the constraint associated with the recombination rate is that the compass starts losing its RF disruption property as the recombination rate is increased. The general trends of the functional window with respect to the hyperfine interaction strength and recombination rates are captured in Fig. 2. The functional window for a few other parameters is also shown in Figs. 5 and 6 (Appendix A). During the exploration of the functional window, the parameter set was narrowed down by setting the requirement for a peak around the geomagnetic field with a functional window as narrow as possible and display of the RF disruption property. The parameter set $(a_x,a_y,a_z,k_s,k_t) = (0.345\ \text{G},0.345\ \text{G},9\ \text{G},2\times10^4\ \text{s}^{-1},2\times10^4\ \text{s}^{-1})$ exhibit both the functional window and the RF disruption property.

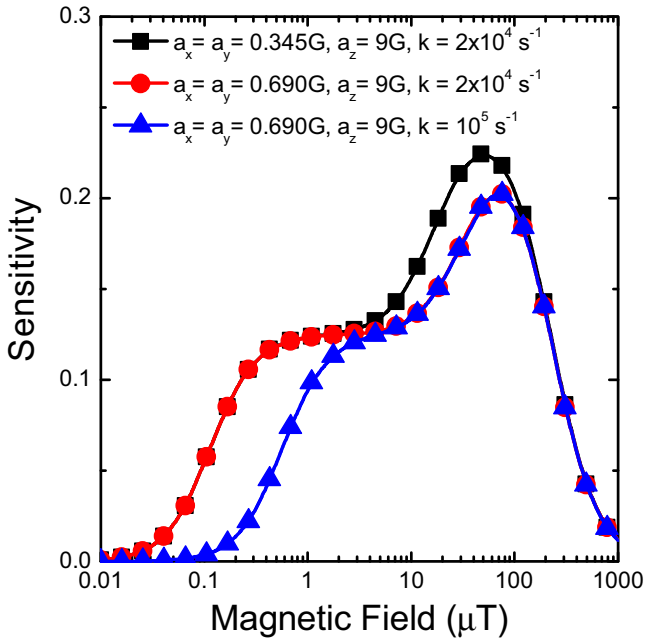

FIG. 2. The general trend of the functional window with hyperfine and recombination rate parameters is shown here. The functional window is plotted for the parameter values of $(a_x,a_y,a_z,k_s,k_t) = (0.345\ \text{G},0.345\ \text{G},9\ \text{G},2\times10^4\ \text{s}^{-1},2\times10^4\ \text{s}^{-1})$, $(0.690\ \text{G},0.690\ \text{G},9\ \text{G},2\times10^4\ \text{s}^{-1},2\times10^4\ \text{s}^{-1})$, and $(0.690\ \text{G}, 0.690\ \text{G},9\ \text{G},10^5\ \text{s}^{-1},10^5\ \text{s}^{-1})$. a_z is kept constant in these plots. The plots show that upon increasing (decreasing) the values of a_x and a_y, the height of the functional window decreases (increases). An increment in the recombination rate shifts the lower portion of the functional window to higher values of the magnetic field.

The analysis suggests that the functional window is observed around the local geomagnetic field if a_x and

a_y are small in comparison to a_z (cigar-shaped hyperfine interaction with $a_x = a_y \ll a_z$). However, if they happen to be vanishingly small ($a_x = a_y \approx 0$), the functional window becomes relatively much broader in the lower magnetic-field regime, something that is not observed in behavioral experiments. For larger values such that $a_x = a_y > a_z$, we still get a functional window but the sensitivity (functional window height) is very small. For still larger values such that $a_x \approx a_y \approx a_z$, the functional window is completely washed out (cf. Fig. 5). In contrast, the functional window turns out to be largely insensitive to the recombination rates—to the extent that increasing or decreasing these (k_s,k_t) up to a factor of 8 with respect to the optimal value does not change the window appreciably. However, this value of recombination rate parameters models the RF disruption appropriately as demonstrated in Fig. 1(b). In Fig. 1(a), we also observe that the RP model can capture the "functional window" behavior qualitatively, but—not unsurprisingly, given its simplicity—is unable even in this best case to reproduce the experimentally observed width and sharpness quantitatively.

We now point out that not only does the essential functional window behavior emerge from the RP model, but so does its adaptation characteristic. Figure 1(c) shows the variation of the center of the functional window for various hyperfine interaction strengths. As the magnitude of the hyperfine interaction (a_z) increases (decreases), the center of the functional window shifts towards higher (lower) magnetic-field values. This observation leads us to conjecture that it is the capability of tuning the functional window that lets the avian compass regain sensitivity when it is subjected to a sudden change in the magnetic field, *viz.*, the functional window adaptation property. Physically, the hyperfine interaction strength has an inverse relation with the distance between nucleus and electron $(1/r^3)$. Therefore, the adaptive behavior here could be realized by small structural adjustments in the radical-pair molecule that modify the hyperfine parameters [36]. We note that while structural deformation is commonplace in molecular and solid-state systems [37–39], making it a plausible mechanism for adaptation, establishing it definitively as the true mechanism would require direct experimental corroboration (there could conceivably be other explanations for the observed behavior of adaptation, e.g., a "learned response" to a changed magnetic field). In order to confirm this, we suggest *in vitro* experiments to directly probe the spin dynamics in cryptochrome or similar organic molecules, perhaps using the ultrasensitive diamond nitrogen-vacancy-center spin system [40]. Finally, the functional window adaptation behavior, like the functional window itself, is again largely insensitive to changes in the recombination rates (k_s,k_t).

As stated above, the RF disruption property was analyzed for various values of recombination rates. Figure 3(a) shows the change in sensitivity as a function of the recombination rate, k (k_s,k_t). It is found that only k_s, k_t values less than 4×10^4 s^{-1} lead to RF disruption in this sense and are, therefore, acceptable from the RP model perspective. From these values of the recombination rate, we conclude that the coherence time of the radical pair must at least be $(4 \times 10^4)^{-1}$ s $= 25$ μs. This rather large time scale seems to corroborate the quantum nature of the avian compass and suggests that it may provide useful learning for quantum technologies.

Next, we analyze the functional window when the recombination rates for the singlet and triplet channels, k_s and k_t, are different. It is usual for these to be considered identical [14,22], but that is actually not to be expected from the physical basis of RP theory. The radical pair can readily recombine back if it happens to be in the singlet state but not from the triplet state, whence it can only form escape products with other species [29]. This suggests that the recombination rate of singlet radical pairs should be taken more than the recombination (or, more accurately, the escape) rate of triplet radical pairs, i.e., $k_s > k_t$. Figure 3(b) shows the functional window behavior of the compass when $k_s > k_t$, with both parameters coming from the range $(k_s,k_t \leqslant 4 \times 10^4$ s$^{-1})$. We observe that the functional window is practically unchanged even when the singlet and triplet recombination times are treated realistically. We point out that the RF disruption property is also preserved as long as k_s and k_t are within the aforementioned range, albeit unequal.

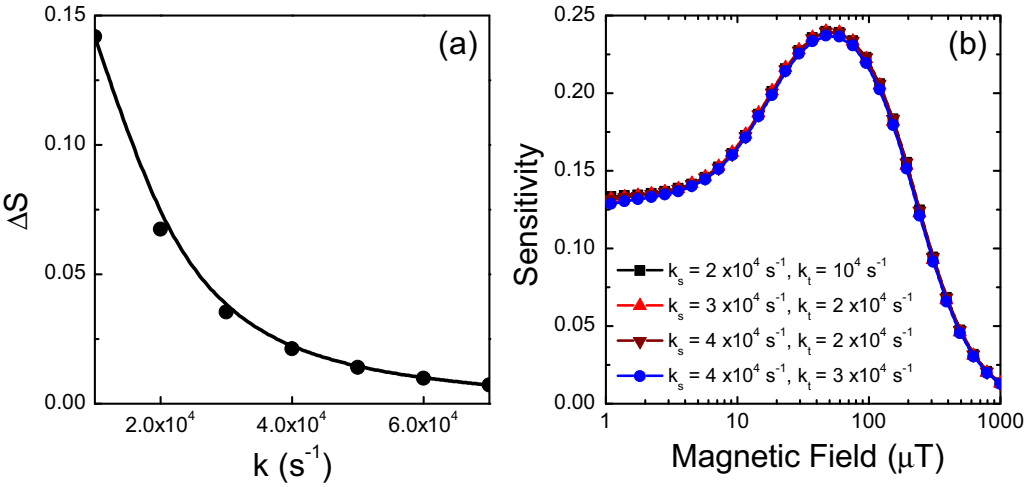

FIG. 3. (a) Change in sensitivity of the compass as a function of the RP recombination rate. (b) Sensitivity as a function of the Zeeman-field strength when singlet and triplet recombination rates are different. We take $k_s > k_t$, which is implied by RP theory [29]. The curve is plotted for $(k_s,k_t) = (2 \times 10^4$ s^{-1},10^4 s^{-1}), $(3 \times 10^4$ s^{-1}, 2×10^4 s^{-1}), $(4 \times 10^4$ s^{-1}, 2×10^4 s^{-1}), and $(4 \times 10^4$ s^{-1}, 3×10^4 s^{-1}).

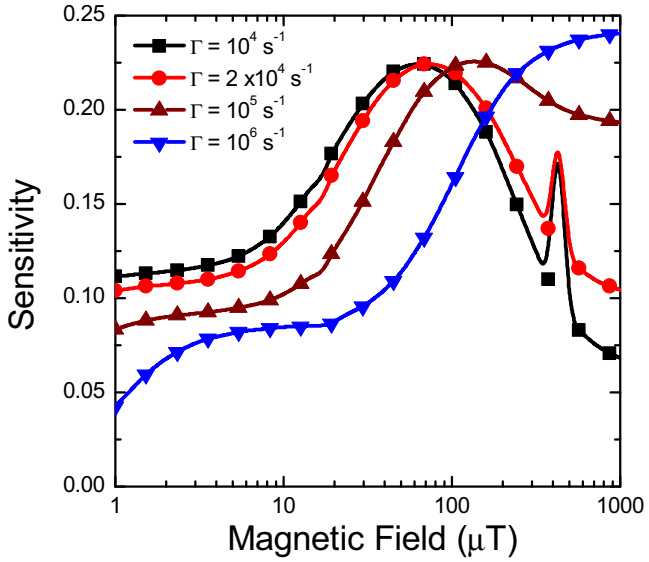

FIG. 4. Compass sensitivity as a function of the Zeeman-field strength in the presence of environmental noise [30]. The sensitivity is analyzed for $(a_x,a_y,a_z,k_s,k_t) = (0.345\ \text{G}, 0.345\ \text{G}, 9\ \text{G}, 2 \times 10^4\ \text{s}^{-1}, 2 \times 10^4\ \text{s}^{-1})$ along with environmental noise rates (Γ) of 10^4, 2×10^4, 10^5, and $10^6\ \text{s}^{-1}$. As is clear, the functional window property vanishes when the noise rate is higher than the RP recombination rate.

Further, we explore the effect of environmental noise on the functional window using a projection noise model [30]. The noise operators are written $L_1 = I_2 \otimes |s\rangle\langle s|$, $L_2 = I_2 \otimes |t_0\rangle\langle t_0|$, $L_3 = I_2 \otimes |t_+\rangle\langle t_+|$, and $L_4 = I_2 \otimes |t_-\rangle\langle t_-|$. The master equation with the inclusion of noise operators reads $\dot{\rho} = -\frac{i}{\hbar}[H,\rho] + k\sum_{i=1}^{8} P_i\rho P_i^\dagger - \frac{1}{2}(P_i^\dagger P_i\rho + \rho P_i^\dagger P_i) + \Gamma\sum_{i=1}^{4} L_i\rho L_i^\dagger - \frac{1}{2}(L_i^\dagger L_i\rho + \rho L_i^\dagger L_i)$, where Γ is the noise rate. Figure 4 shows the functional window for $(a_x,a_y,a_z,k) = (0.345\ \text{G}, 0.345\ \text{G}, 9\ \text{G}, 2 \times 10^4\ \text{s}^{-1})$ in the presence of noise rates of 10^4, 2×10^4, 10^5, and $10^6\ \text{s}^{-1}$. Expectedly, it shows that the functional window vanishes for noise rates that are larger than the recombination rate(s). We note the presence of small spikes in the sensitivity beyond the main peak for small values of the noise rate. Whether these have any special significance [31] is not clear to us at this point. In Appendix B, we explore the functional window behavior with another noise model [14] that is more detrimental to the compass sensitivity (cf. Fig. 7).

IV. DISCUSSION

So far we have shown that the functional window and its adaptation property can be explained within the RP model. However, the following fundamental question is left open: What purpose, if any, does the functional window of the avian compass actually serve? In fact, the role of the geomagnetic field as an abiotic evolutionary force remains largely unexplored. Here we make the provisional assumption that magnetoreception itself might be providing some evolutionary benefit by aiding migration and, thereafter, examine whether a functional window therein brings any further advantage. We first consider an apparently plausible evolutionary purpose for the large-field (right-hand) side of the window, *viz.*, to protect this magnetic-field sensor from large stray magnetic fields and fluctuations. However, major fluctuations like solar flares that do disorient certain bird species [41,42] have very low amplitudes; it is likely that the disruption in fact occurs via its RF disruption property [18]. On the other hand, spatial (pole-equator) and temporal (e.g., secular, i.e., roughly annual) variations of the geomagnetic field—which birds obviously need to be able to sense—are actually larger than the experimentally observed functional window [43]. All things considered, it then seems plausible that the functional window is an incidental feature, a by-product, of the RP spin dynamics, with no obvious evolutionary benefit (we note that the question of evolutionary benefit has come up for debate in other areas of quantum biology as well [7,36,44]). Now, given the overly narrow functional window, its adaptation property seems necessary to accommodate variations of the geomagnetic field; and, as we have seen earlier, adaptation could also emerge as a corollary of the RP dynamics. In fact, the centering of the functional window on the local and present geomagnetic field points to some built-in mechanism for adaptation.

We would like to point out that the simple RP model—despite its success in explaining behavioral observations—is not quantitatively accurate and, hence, cannot be considered complete yet; when it is, the experimentally observed sharp functional window should emerge from the RP spin dynamics itself. We note here that we attempted to generalize the RP model by incorporating spin-spin interactions, namely, exchange and dipolar, but found that these do not help to model the sharpness of the functional window; this agrees with earlier model predictions that the RP spin dynamics is robust against such external interactions [45,46]. In turn, this means that hybrid mechanisms, combining RP and magnetic particles [47,48], would also not materially affect the functional window. We feel that the necessary generalization of the RP model could be along two dimensions: (i) in terms of subtle environmental interaction, which has a well-known precedent in quantum biology [2,49]; and (ii) the addition of more nuclei contributing to the hyperfine interaction with the radical pair, which would be a more realistic model for cryptochrome [16]. On the question of the evolutionary benefits of the functional window and, more generally, avian magnetoreception itself: A good starting point seems to be a correlation of geomagnetic-field variation with the evolution of cryptochrome or, in general, the magnetoreception capability in birds. Finally, this domain would also benefit immensely from direct, possibly *in vitro*, experimental observation of cryptochrome spin dynamics—going beyond the behavioral experiments that we rely on exclusively today.

V. CONCLUSION

In conclusion, we have shown that the qualitative characteristics of the avian compass emerge from the RP model with biologically feasible parameters. We have specifically shown that the functional window behavior can be accounted for within the RP model. However, the one-nucleus radical-pair model cannot capture the experimental sharpness of the functional window. We conjecture that this may be a shortcoming of the way that environmental interactions have been

modeled so far and may be addressed by considering realistic numbers of nuclei in the model. We further observe that the behavioral property of adaptation (to a different Zeeman field) can also be accounted for within the RP model through moderate tuning of the hyperfine parameters. The same hyperfine parameters together with appropriate recombination parameters also lead to the RF disruption property of the avian compass—which is found to be more sensitive to the latter. The functional window, on the other hand, is found to be generally insensitive to variation of recombination rates and to unequal singlet and triplet recombination rates. The recombination rates, however, are essential in setting the coherence time for the system, which in turn determines the level of environmental noise it can withstand. We show that for noise rates higher than the recombination rate, the functional window vanishes. Finally, we observe that even if we assume evolutionary benefits accruing to bird species from RP magnetoreception, there is no clear biological raison d'être to have a functional window therein; thus, it could simply be a by-product of the RP spin dynamics, with no utilitarian role per se.

ACKNOWLEDGMENTS

We are grateful for the support from the Ministry of Electronics and Information Technology, Government of India through the Centre of Excellence in Nanoelectronics at IIT Bombay.

APPENDIX A: FUNCTIONAL WINDOW AT VARIOUS HYPERFINE AND RECOMBINATION RATE VALUES

In the text, we have shown the functional window for a one-nucleus radical-pair system for hyperfine and recombination parameter values of $(a_x,a_y,a_z,k_s,k_t) = (0.345\ \text{G},0.345\ \text{G},9\ \text{G},2\times10^4\ \text{s}^{-1},2\times10^4\ \text{s}^{-1})$. We have analyzed the compass sensitivity as a function of the geomagnetic field strength for a very large number of parameters. Upon close inspection of the results, a pattern in the functional window is observed. It is discussed in the text (cf. Sec. III). Here, in Fig. 5, we show the compass sensitivity for a few other parameter values from different parameter regimes to clarify the assertions made there. In Fig. 5, the compass sensitivity has been plotted for parameter values of $(a_x, a_y,a_z,k\ (=k_s=k_t)) = (0.345\ \text{G},0.345\ \text{G},1\ \text{G},2\times10^4\ \text{s}^{-1})$, $(0\ \text{G},0\ \text{G},1\ \text{G},5\times10^4\ \text{s}^{-1})$, $(9\ \text{G},9\ \text{G},9\ \text{G},2\times10^4\ \text{s}^{-1})$, and $(18.80\ \text{G},37.60\ \text{G},0\ \text{G},5\times10^5\ \text{s}^{-1})$. We can draw the following conclusions from Fig. 5: (a) There is a parameter regime where the functional-window-like behavior is not observable. It is shown in the figure for the parameter values $(a_x,a_y,a_z,k) = (9\ \text{G},9\ \text{G},9\ \text{G},2\times10^4\ \text{s}^{-1})$ and $(18.80\ \text{G},37.60\ \text{G},0\ \text{G},5\times10^5\ \text{s}^{-1})$; (b) The radical-pair model exhibits the functional window for a few parameter values but the window is too broad compared to the one reported in Fig. 1; it is demonstrated in Fig. 5 for parameter values of $(a_x,a_y,a_z,k) = (0.345\ \text{G},0.345\ \text{G},1\ \text{G},2\times10^4\ \text{s}^{-1})$. Here the functional window has a much lower magnitude too. The functional window for $(a_x,a_y,a_z,k) = (0.345\ \text{G},0.345\ \text{G},1\ \text{G},2\times10^4\ \text{s}^{-1})$ shows a peak in the sensitivity in addition to the functional-window-like behavior. (c) For a few parameters, the sensitivity plot has a nontrivial shape showing multiple peaks even in the absence of any environmental noise. This is shown in Fig. 5 for parameter values of $(a_x,a_y,a_z,k) = (0\ \text{G},0\ \text{G},1\ \text{G},5\times10^4\ \text{s}^{-1})$.

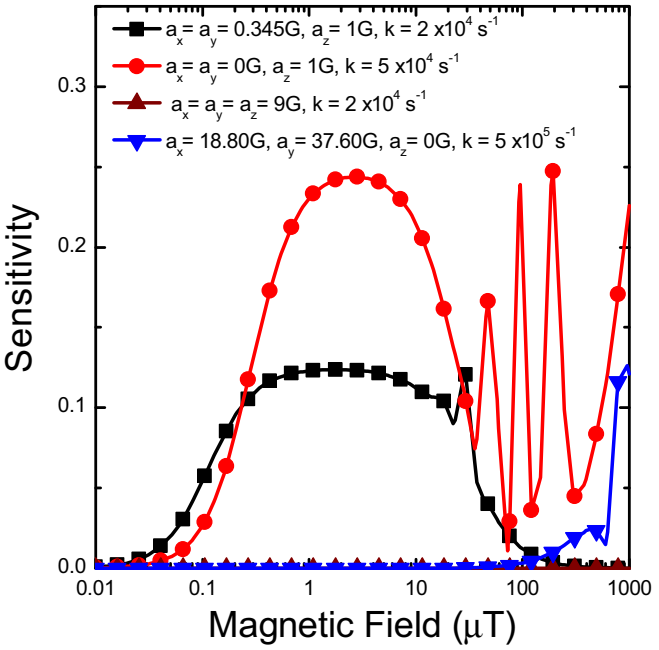

FIG. 5. Compass sensitivity as a function of the Zeeman field for various hyperfine and recombination rate parameters. The sensitivity is plotted for $(a_x,a_y,a_z,k\ (=k_s,k_t)) = (0.345\ \text{G},0.345\ \text{G},1\ \text{G},2\times10^4\ \text{s}^{-1})$, $(0\ \text{G},0\ \text{G},1\ \text{G},5\times10^4\ \text{s}^{-1})$, $(9\ \text{G},9\ \text{G},9\ \text{G},2\times10^4\ \text{s}^{-1})$, and $(18.80\ \text{G},37.60\ \text{G},0\ \text{G},5\times10^5\ \text{s}^{-1})$. The plot intends to show the sensitivity behavior for parameters other than the ones mentioned in the text.

In addition to various hyperfine interaction strength parameters, to demonstrate the effect of increasing the recombination rate from its value of $2\times10^4\ \text{s}^{-1}$, we analyze the compass sensitivity as a function of the geomagnetic-field strength for several values of recombination rate $k\ (=k_s=k_t)$. The plot is shown in Fig. 6. The compass sensitivity is plotted for $k = 10^5$, 10^6, 10^7, and $10^8\ \text{s}^{-1}$ with $(a_x,a_y,a_z) = (0.345\ \text{G},0.345\ \text{G},9\ \text{G})$. Figure 6 clearly shows that as the recombination rate is increased beyond $10^6\ \text{s}^{-1}$, the functional-window-like behavior of the radical pair ceases to exist. We still observe a functional window for $k = 10^5\ \text{s}^{-1}$. For higher values of the recombination rate, the radical pair does not get enough time for interstate transitions in order to have appreciable sensitivity [31].

APPENDIX B: EFFECT OF ENVIRONMENTAL NOISE ON THE FUNCTIONAL WINDOW

In the text, we show the effect of noise on the functional window (cf. Fig. 4). The noise model considered there is projection noise [30]. Here we consider another noise model, taken from Ref. [14], and analyze its effect on the functional window. The noise operators in this case are given as $L_1 = I_2\otimes\sigma_x\otimes I_2$, $L_2 = I_2\otimes\sigma_y\otimes I_2$, $L_3 = I_2\otimes\sigma_z\otimes I_2$, $L_4 = I_2\otimes I_2\otimes\sigma_x$, $L_5 = I_2\otimes I_2\otimes\sigma_y$, and $L_6 = I_2\otimes I_2\otimes\sigma_z$. This type of noise opens the spin transition pathways between all spin states (singlet and

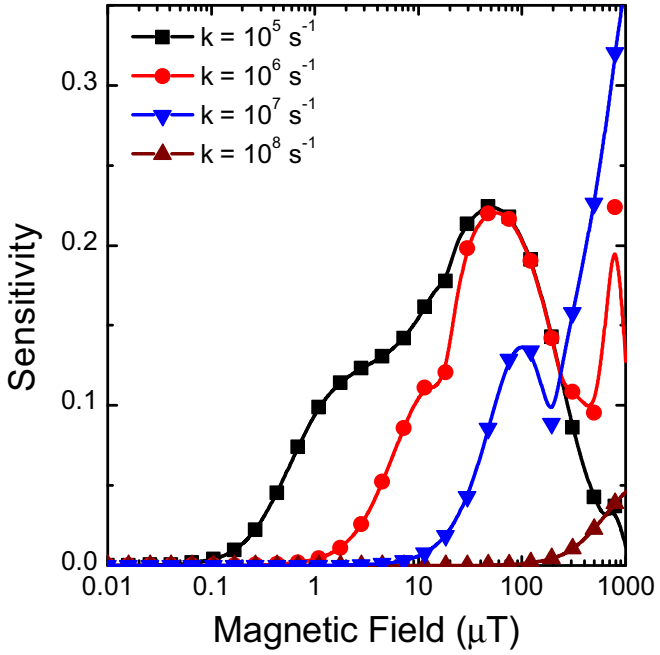

FIG. 6. Compass sensitivity as a function of the Zeeman field for $(a_x,a_y,a_z) = (0.345\ \text{G}, 0.345\ \text{G}, 9\ \text{G})$ and recombination rates of $k = (10^5\ \text{s}^{-1}, 10^6\ \text{s}^{-1}, 10^7\ \text{s}^{-1}, 10^8\ \text{s}^{-1})$. The plot shows the change in the functional window property of the avian compass when the recombination rate is increased. We observe that the functional window property starts to become distorted when the recombination rate is increased beyond $10^6\ \text{s}^{-1}$. The functional window becomes nonexistent for $k = 10^7\ \text{s}^{-1}$ and $k = 10^8\ \text{s}^{-1}$.

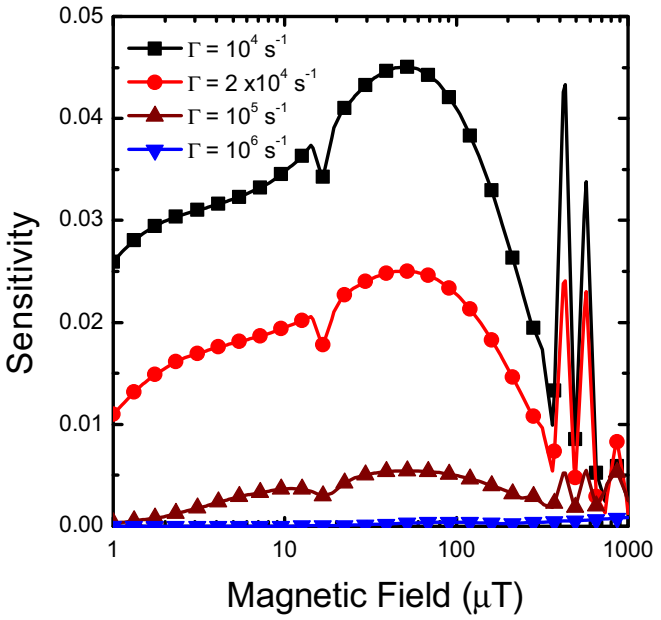

FIG. 7. Compass sensitivity as a function of the Zeeman-field strength in the presence of environmental noise [14]. The sensitivity is plotted for $(a_x,a_y,a_z,k_s,k_t) = (0.345\ \text{G}, 0.345\ \text{G}, 9\ \text{G}, 2\times 10^4\ \text{s}^{-1}, 2\times 10^4\ \text{s}^{-1})$ along with environmental noise rates (Γ) of 10^4, 2×10^4, 10^5, and $10^6\ \text{s}^{-1}$. The sensitivity in this case is much lower than that is for the noise model used in the text (cf. Fig. 4).

triplets) and, hence, makes the singlet yield uniform with respect to the magnetic-field inclination. Consequently, the sensitivity is much lower than that is for the other noise model. This fact is also evident in Fig. 7, where we plot the compass sensitivity as a function of the geomagnetic-field strengths for noise rates of 10^4, 2×10^4, 10^5, and $10^6\ \text{s}^{-1}$. This type of noise kills the sensitivity of the compass. Hence, the higher the noise rate, the lower is the sensitivity.

[1] G. S. Engel, T. R. Calhoun, E. L. Read, T.-K. Ahn, T. Mančal, Y.-C. Cheng, R. E. Blankenship, and G. R. Fleming, Nature **446**, 782 (2007).

[2] M. B. Plenio and S. F. Huelga, New J. Phys. **10**, 113019 (2008).

[3] F. Levi, S. Mostarda, F. Rao, and F. Mintert, Rep. Prog. Phys. **78**, 082001 (2015).

[4] L. Turin, Chem. Senses **21**, 773 (1996).

[5] J. C. Brookes, F. Hartoutsiou, A. P. Horsfield, and A. M. Stoneham, Phys. Rev. Lett. **98**, 038101 (2007).

[6] D. Polli, P. Altoè, O. Weingart, K. M. Spillane, C. Manzoni, D. Brida, G. Tomasello, G. Orlandi, P. Kukura, R. A. Mathies *et al.*, Nature **467**, 440 (2010).

[7] Z. D. Nagel and J. P. Klinman, Chem. Rev. **106**, 3095 (2006).

[8] H. B. Gray and J. R. Winkler, Q. Rev. Biophys. **36**, 341 (2003).

[9] N. Lambert, Y.-N. Chen, Y.-C. Cheng, C.-M. Li, G.-Y. Chen, and F. Nori, Nat. Phys. **9**, 10 (2013).

[10] M. Mohseni, Y. Omar, G. S. Engel, and M. B. Plenio, *Quantum Effects in Biology* (Cambridge University Press, Cambridge, UK, 2014).

[11] T. Ritz, S. Adem, and K. Schulten, Biophys. J. **78**, 707 (2000).

[12] I. K. Kominis, Phys. Rev. E **80**, 056115 (2009).

[13] J. Cai, G. G. Guerreschi, and H. J. Briegel, Phys. Rev. Lett. **104**, 220502 (2010).

[14] E. M. Gauger, E. Rieper, J. J. L. Morton, S. C. Benjamin, and V. Vedral, Phys. Rev. Lett. **106**, 040503 (2011).

[15] M. Tiersch and H. J. Briegel, Philos. Trans. Roy. Soc. A: Math. Phys. Eng. Sci. **370**, 4517 (2012).

[16] H. G. Hiscock, S. Worster, D. R. Kattnig, C. Steers, Y. Jin, D. E. Manolopoulos, H. Mouritsen, and P. Hore, Proc. Natl. Acad. Sci. USA **113**, 4634 (2016).

[17] K. Schulten, C. E. Swenberg, and A. Weller, Z. Phys. Chem. **111**, 1 (1978).

[18] T. Ritz, P. Thalau, J. B. Phillips, R. Wiltschko, and W. Wiltschko, Nature **429**, 177 (2004).

[19] P. Thalau, T. Ritz, K. Stapput, R. Wiltschko, and W. Wiltschko, Naturwissenschaften **92**, 86 (2005).

[20] T. Ritz, R. Wiltschko, P. Hore, C. T. Rodgers, K. Stapput, P. Thalau, C. R. Timmel, and W. Wiltschko, Biophys. J. **96**, 3451 (2009).

[21] R. Wiltschko, P. Thalau, D. Gehring, C. Nießner, T. Ritz, and W. Wiltschko, J. R. Soc. Interface **12**, 20141103 (2015).

[22] J. N. Bandyopadhyay, T. Paterek, and D. Kaszlikowski, Phys. Rev. Lett. **109**, 110502 (2012).
[23] W. Wiltschko and R. Wiltschko, Science **176**, 62 (1972).
[24] W. Wiltschko, in *Animal Migration, Navigation, and Homing. Proceedings in Life Sciences*, edited by K. Schmidt-Koenig and W. T. Keeton (Springer, Berlin, 1978), pp. 302–310.
[25] M. Winklhofer, E. Dylda, P. Thalau, W. Wiltschko, and R. Wiltschko, Proc. R. Soc. London B **280**, 20130853 (2013).
[26] C. T. Rodgers and P. J. Hore, Proc. Natl. Acad. Sci. USA **106**, 353 (2009).
[27] W. Wiltschko, R. Wiltschko, and T. Ritz, Procedia Chem. **3**, 276 (2011).
[28] B.-M. Xu, J. Zou, J.-G. Li, and B. Shao, Phys. Rev. E **88**, 032703 (2013).
[29] J. C. S. Lau, D.Phil. thesis, University of Oxford, 2014.
[30] Z. B. Walters, Phys. Rev. E **90**, 042710 (2014).
[31] V. S. Poonia, D. Saha, and S. Ganguly, Phys. Rev. E **91**, 052709 (2015).
[32] H. J. Hogben, O. Efimova, N. Wagner-Rundell, C. R. Timmel, and P. Hore, Chem. Phys. Lett. **480**, 118 (2009).
[33] J. Cai, F. Caruso, and M. B. Plenio, Phys. Rev. A **85**, 040304(R) (2012).
[34] C. Timmel, U. Till, B. Brocklehurst, K. McLauchlan, and P. Hore, Mol. Phys. **95**, 71 (1998).
[35] J. Johansson, P. Nation, and F. Nori, Comput. Phys. Commun. **184**, 1234 (2013).
[36] S. F. Huelga and M. B. Plenio, Contemp. Phys. **54**, 181 (2013).
[37] A. M. Berghuis and G. D. Brayer, J. Mol. Biol. **223**, 959 (1992).
[38] M. Kondoh, C. Shiraishi, P. Müller, M. Ahmad, K. Hitomi, E. D. Getzoff, and M. Terazima, J. Mol. Biol. **413**, 128 (2011).
[39] M. Sturge, Solid State Phys. **20**, 91 (1968).
[40] H. Liu, M. B. Plenio, and J. Cai, Phys. Rev. Lett. **118**, 200402 (2017).
[41] Bilco, http://www.pigeonbasics.com/articles/article2.html, Accessed: 13 July 2015.
[42] http://solar-center.stanford.edu/solar-weather/pigeons.html, Accessed: 13 July 2015.
[43] A. Cox and R. R. Doell, Geol. Soc. Am. Bull. **71**, 645 (1960).
[44] P. Ball, Nature **431**, 396 (2004).
[45] O. Efimova and P. Hore, Biophys. J. **94**, 1565 (2008).
[46] A. Dellis and I. Kominis, Biosystems **107**, 153 (2012).
[47] S. Qin, H. Yin, C. Yang, Y. Dou, Z. Liu, P. Zhang, H. Yu, Y. Huang, J. Feng, J. Hao *et al.*, Nat. Mater. **15**, 217 (2016).
[48] K. J. Lohmann, Nat. Mater. **15**, 136 (2016).
[49] A. W. Chin, A. Datta, F. Caruso, S. F. Huelga, and M. B. Plenio, New J. Phys. **12**, 065002 (2010).